IEEE Access
Multidisciplinary | Rapid Review | Open Access Journal

Received September 23, 2021, accepted October 14, 2021, date of publication October 18, 2021, date of current version October 29, 2021.

Digital Object Identifier 10.1109/ACCESS.2021.3121280

Three-Dimensional Magnetic Hysteresis Modeling Based on Vector Hysteresis Operator

DANDAN LI[1], ZHENYANG QIAO[2], YUXIANG WU[1], ZHONGKANG LI[1], YINMAO SONG[1], AND YONGJIAN LI[3], (Member, IEEE)

[1]Henan Engineering Research Center for Intelligent Buildings and Human Settlements, School of Building Environment Engineering, Zhengzhou University of Light Industry, Zhengzhou 450001, China
[2]School of Mechatronic Engineering and Automation, Shanghai University, Shanghai 200444, China
[3]State Key Laboratory of Reliability and Intelligence of Electrical Equipment, Hebei University of Technology, Tianjin 300130, China

Corresponding author: Dandan Li (lidandan@zzuli.edu.cn)

This work was supported in part by the National Natural Science Foundation of China under Grant 51607157 and Grant 51777055, and in part by the Doctor Foundation of Zhengzhou University of Light Industry, Zhengzhou, Henan, China, under Grant 2015BSJJ012.

ABSTRACT Based on the minimum energy principle of magnetization stable state, this paper presents a definition of three-dimensional (3-D) hysteresis operator by analyzing the magnetization state of the magnetic particles. The direction determination rule of magnetization is given in detail. The critical surface equation of the hysteresis operator is described in the space sphere coordinate system according to the modeling principle of the hybrid vector hysteresis model. The magnetization process of the hysteresis operator is studied under the alternating and rotational magnetic field, respectively. Moreover, a 3-D isotropic hysteresis model is initiatively established, and the hysteresis properties of soft magnetic composite (SMC) material are simulated and compared with the experimental results. This study lays a foundation to build the 3-D hybrid vector hysteresis model and simulate the 3-D magnetic properties.

INDEX TERMS Magnetic hysteresis model, hysteresis operator, hysteresis properties.

I. INTRODUCTION

Modeling of magnetic properties is a hot topic in the field of electrical engineering. Preisach model, Jiles-Atherton (J-A) model, Stoner-Wohlfarth (S-W) model and Enokizono, and Soda (E&S) model *et al.* are typical modeling methods for magnetic properties study at present. [1]–[8] Each model has its characteristics and applicable occasions in different ways.

After years of development, the research on these models can be divided into three categories: scalar hysteresis model, vector hysteresis model, and hybrid vector hysteresis model. The scalar model is essentially a special case of the vector model. The hybrid hysteresis model combining two or more basic models has attracted the attention of scholars recently. It combines the advantages of the basic models, while avoids disadvantages, which can simulate the hysteresis properties more accurately. The idea of the hybrid vector hysteresis model was proposed earlier by G. Friedman and I. D. Mayergoyz. [9] It was derived from a general vector Preisach model by extending the S-W model and Mayergoyz's vector Preisach model. C. Michelakis *et al.* proposed a hybrid vector hysteresis model for single domain single axis particles by combining the classical Preisach model and S-W model [10], [11 E. Della Torre and E. Cardelli presented the general vector hysteresis model (GHM, Generalized hysteresis model) and DPC (Della Torre, Pinzaglia and Cardelli) model. The GHM model calculates the irreversible magnetization components based on the closed critical surface of each hysteresis operator [12]–[14] While the DPC model can analyze the magnetization characteristics of unit single domain particles [15]–[17] Dingsheng Lin *et al.* presented an anisotropic vector hysteresis model based on the improved isotropic vector play operators [18].

The author's research group has been keen on the study in the field of hysteresis characteristic simulation. The definition method of vector hysteresis operator was presented and a 2-D vector hysteresis mathematical model was established to simulate the hysteresis characteristic for soft magnetic composites in previous publications [19]–[21] On the basis of the results of previous research, a definition of hysteresis operator in 3-D case is proposed and expanded in detail in this paper. The magnetization state of magnetic particles is analyzed based on the principle of minimum energy of magnetized stable state. According to the astroid

The associate editor coordinating the review of this manuscript and approving it for publication was Michail Makridis.

properties, the 3-D hysteresis operators are established for anisotropic and isotropic materials in the spherical coordinate system, respectively. Meanwhile, the influence of the energy parameter on the critical surface of the hysteresis operator is analyzed. And then, the magnetization process of hysteresis operator is studied under alternating and rotational magnetic field. Finally, a 3-D isotropic hysteresis model is preliminarily established based on the 3-D hysteresis operator. The hysteresis properties of SMC material are simulated and compared with the experimental data to verify the availability of the 3-D model.

II. ANALYSIS OF MAGNETIZATION STATE OF MAGNETIC PARTICLES

According to the minimum energy principle of magnetization stable state, the magnetization state of magnetic particles is analyzed. In the case of single domain single axis anisotropic particles, the direction of the magnetization is consistent with the easy axis direction under zero magnetic field. After applying the field, the direction of the magnetization is rotated off the easy axis towards the direction of the applied magnetic field. The vector magnetization $\boldsymbol{M}$, applied magnetic field $\boldsymbol{H}_a$, and their projections on the *xoy* plane are shown in Fig. 1.

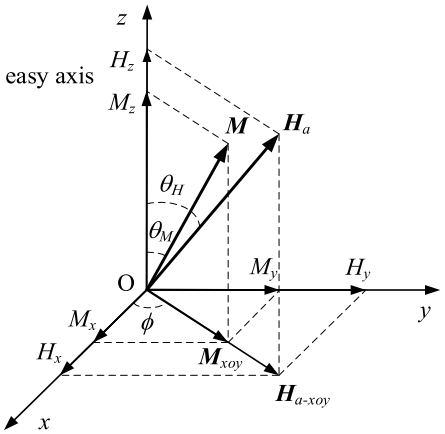

FIGURE 1. Relationship between $\boldsymbol{M}$, $\boldsymbol{H_a}$, and their projections on the *xoy* plane.

In Fig. 1, z axis is assumed to be the easy axis, θ_M is the angle between $\boldsymbol{M}$ and z axis, θ_H is the angle between $\boldsymbol{H}_a$ and z axis, and ϕ is the angle between $\boldsymbol{M}_{xoy}$ or $\boldsymbol{H}_{a-xoy}$(the projection of $\boldsymbol{M}$ or $\boldsymbol{H}_a$ on the *xoy* plane) and the x axis.

The total free energy E of the single domain single axis anisotropic particles with volume V is equal to the sum of uniaxial anisotropic energy and field energy, see (1).

$$E = V[K\sin^2\theta_M - u_0\boldsymbol{M}\cdot\boldsymbol{H}_a] \tag{1}$$

where K is the anisotropy coefficient.

The formula $\boldsymbol{m} = \boldsymbol{M}\,/\,M_s$ is used for normalizing $\boldsymbol{M}$, where $\boldsymbol{m}$ is the unit vector magnetization and its modulus is 1. The coordinate algorithm of vector dot product is used to transform (1) to (2).

$$E = V[K\sin^2\theta_M - \mu_0 M_s H_a(\sin\theta_M\cos\phi\sin\theta_H\cos\phi + \sin\theta_M\sin\phi\sin\theta_H\sin\phi + \cos\theta_M\cos\theta_H)] \tag{2}$$

Equation (3) can be obtained by using $e_0 = E/2KV$, $h_a = \mu_0 M_s H_a/2K$, and the components of h_a along the coordinate axis to simplify (2).

$$e_0 = \frac{1}{2}\sin^2\theta_M - h_x\sin\theta_M\cos\phi - h_y\sin\theta_M\sin\phi - h_z\cos\theta_M \tag{3}$$

According to the principle of minimum energy, the energy parameter e_0 must satisfy (4).

$$\begin{cases}\dfrac{\partial e_0}{\partial\theta_M} = 0\\ \dfrac{\partial^2 e_0}{\partial\theta_M^2} > 0\end{cases} \tag{4}$$

Assuming neither $\sin\theta_M$ nor $\cos\theta_M$ is 0, so (5) can be deduced from $\partial e_0/\,\partial\theta_M = 0$.

$$\frac{h_x\cos\phi + h_y\sin\phi}{\sin\theta_M} - \frac{h_z}{\cos\theta_M} = 1 \tag{5}$$

The (6) can be obtained by calculating $\partial e_0/\,\partial\phi = 0$.

$$\begin{cases}h_x = h_y\cot\phi\\ h_y = h_x\tan\phi\end{cases} \tag{6}$$

Equation (6) can also be directly derived from Fig. 1.

The relationship among h_x, h_y and h_z can be derived by (5) and (6), see (7).

$$\begin{cases}h_x = \left(\dfrac{h_z}{\cos\theta_M} + 1\right)\sin\theta_M\cos\phi\\ h_y = \left(\dfrac{h_z}{\cos\theta_M} + 1\right)\sin\theta_M\sin\phi\end{cases} \tag{7}$$

Equation (8) can be deduced from $\partial^2 e_0/\,\partial\theta_M^2 > 0$

$$\frac{h_z + \cos^3\theta_M}{\cos\theta_M} > 0 \tag{8}$$

When the energy is taken to the extreme value, the critical surface can be described as (9), and the corresponding critical surface named 3-D astroid surface is shown in Fig. 2.

$$\begin{cases}h_x = \sin^3\theta_M\cos\phi\\ h_y = \sin^3\theta_M\sin\phi\\ h_z = -\cos^3\theta_M\end{cases} \tag{9}$$

Substituting h_x, h_y and h_z into (3) respectively, and the equation of equipotential surface can be calculated from $\mathrm{d}e_0 = 0$, see (10). Where e is the energy parameter.

$$\begin{cases}h_x = \left[-\dfrac{1}{2}\sin^3\theta_M + (1-e)\sin\theta_M\right]\cos\phi\\ h_y = \left[-\dfrac{1}{2}\sin^3\theta_M + (1-e)\sin\theta_M\right]\sin\phi\\ h_z = \dfrac{1}{2}\cos^3\theta_M - \left(\frac{1}{2}+e\right)\cos\theta_M\end{cases} \tag{10}$$

As shown in Fig. 1 and (10), when $\theta_M = -\pi/2$, 0, $\pi/2$, and π, the surface formed by the equation cannot form a closed surface, none of them satisfies the requirements of

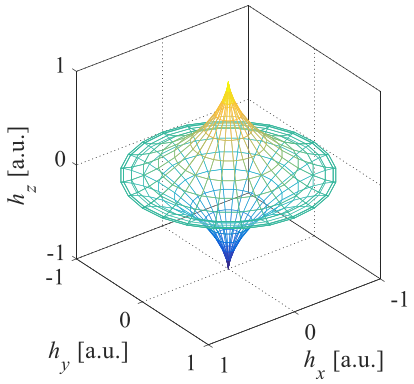

FIGURE 2. The 3-D astroid surface.

establishing 3-D hysteresis operator. Therefore, neither $\sin\theta_M$ nor $\cos\theta_M$ is 0, which also verifies the assumption.

According to (8) and (10), it is known that all points on the equipotential surface are in a stable state when $e < -0.5$.

And when the effect of anisotropic constant is considered, (11) can be obtained by using $e_0 = E/2V$, $h_a = \mu_0 M_s H_a/2$, and dividing h_a into three axes to simplify (2).

$$e_0 = \frac{K}{2}\sin^2\theta_M - h_x\sin\theta_M\cos\phi - h_y\sin\theta\sin\phi - h_z\cos\theta_M \tag{11}$$

The 3-D astroid surface can also be obtained when the energy is taken to the extreme value, see (12) and Fig. 3.

$$\begin{cases} h_x = K\sin^3\theta_M\cos\phi \\ h_y = K\sin^3\theta_M\sin\phi \\ h_z = -K\cos^3\theta_M \end{cases} \tag{12}$$

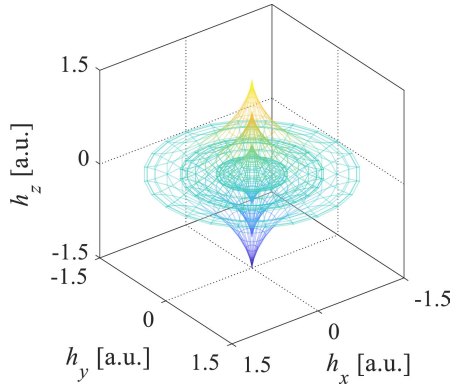

FIGURE 3. 3-D astroid surface when $K = 0.5, 1, 1.5$.

And the equation of equipotential surface can be calculated from $de_0 = 0$, see (13).

$$\begin{cases} h_x = \left[-\frac{K}{2}\sin^3\theta_M + (K-e)\sin\theta_M\right]\cos\phi \\ h_y = \left[-\frac{K}{2}\sin^3\theta_M + (K-e)\sin\theta_M\right]\sin\phi \\ h_z = \frac{K}{2}\cos^3\theta_M - \left(\frac{K}{2}+e\right)\cos\theta_M \end{cases} \tag{13}$$

It is also known that all points on the equipotential surface are in a stable state when $e < -(K/2)$. If the anisotropic constant is not considered, it is the same situation as taking the anisotropic coefficient K to 1, this paper takes $K = 1$.

In the same way, the magnetization state of isotropic magnetic particles is analyzed, too. The total free energy of the single domain single axis isotropic particles can be equal to the field energy, see (14).

$$E = -\mu_0 \boldsymbol{M}\cdot\boldsymbol{H}_a \tag{14}$$

The formula $\boldsymbol{m} = \boldsymbol{M}/M_s$ is used for normalizing $\boldsymbol{M}$, where $\boldsymbol{m}$ is the unit vector magnetization and its modulus is 1. The coordinate algorithm of the vector dot product is used to transform (14) to (15).

$$\begin{aligned} E = -\mu_0 M_s H_a(&\sin\theta_M\cos\phi\sin\theta_H\cos\phi \\ &+\sin\theta_M\sin\phi\sin\theta_H\sin\phi + \cos\theta_M\cos\theta_H) \end{aligned} \tag{15}$$

By using $e_0 = E/2$, $h_a = \mu_0 M_s H_a/2$ and dividing h_a into three axes, (15) can be simplified.

$$e_0 = -h_x\sin\theta_M\cos\phi - h_y\sin\theta_M\sin\phi - h_z\cos\theta_M \tag{16}$$

Samely, the energy parameter e_0 must satisfy (4). It can be also assumed that neither $\sin\theta_M$ nor $\cos\theta_M$ is 0, so (17) can be derived from $\partial e_0/\partial\theta_M = 0$.

$$\frac{h_x\cos\phi + h_y\sin\phi}{\sin\theta_M} - \frac{h_z}{\cos\theta_M} = 0 \tag{17}$$

Equation (18) can be obtained by calculating $\partial e_0/\partial\phi = 0$ (or directly derived from Fig. 1).

$$\begin{cases} h_x = h_y\cot\phi \\ h_y = h_x\tan\phi \end{cases} \tag{18}$$

The relationship among h_x, h_y, and h_z can be derived by (17) and (18), see (19).

$$\begin{cases} h_x = \dfrac{h_z}{\cos\theta_M}\sin\theta_M\cos\phi \\ h_y = \dfrac{h_z}{\cos\theta_M}\sin\theta_M\sin\phi \end{cases} \tag{19}$$

Equation (20) can be deduced from $\partial^2 e_0/\partial\theta_M^2 > 0$.

$$\frac{h_z}{\cos\theta_M} > 0 \tag{20}$$

Substituting h_x, h_y and h_z into (16) respectively, and the equation of equipotential surface can be got from $de_0 = 0$, see (21).

$$\begin{cases} h_x = -e\sin\theta_M\cos\phi \\ h_y = -e\sin\theta_M\sin\phi \\ h_z = -e\cos\theta_M \end{cases} \tag{21}$$

As can be seen from Fig. 1 and (21), when $\theta_M = -\pi/2, 0, \pi/2$ and π, the surface formed by the equation is not closed, so they cannot satisfy the requirements of establishing 3-D hysteresis operator. Therefore, neither $\sin\theta_M$ nor $\cos\theta_M$ is 0, it also verifies the assumption.

According to (20) and (21), all points on the equipotential surface are testified in a stable state when $e < 0$.

III. DEFINITION OF HYSTERESIS OPERATOR IN 3-D CASE

The definition of hysteresis operator plays a very important role in the vector hysteresis modeling and can be concluded from the previous study. The magnetization direction of the points on the equipotential surface in the stable state satisfies the astroid properties of the S-W model [17], [19]–[21] The direction of spontaneous magnetization should satisfy the principle of minimum energy in S-W model. The principle of hysteresis operator definition is to make the magnetization direction easy to be determined and the numerical realization of the whole model simple and feasible.

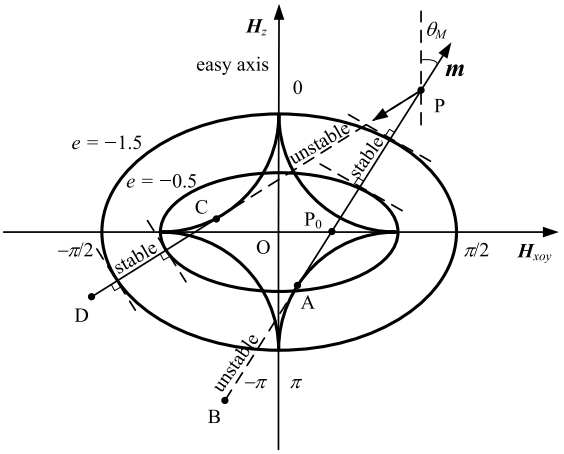

FIGURE 4. Determination of the magnetization direction.

Here, the equation of equipotential surface in stable state is selected as the critical surface of hysteresis operator. The reason why hysteresis operator is defined in this way and the determination of magnetization direction are analyzed as follows. The determination of the magnetization direction is shown in Fig. 4.

In (5), the magnetic force line satisfies (22).

$$h_{xoy} = h_z \tan\theta_M + \sin\theta_M \tag{22}$$

Then, (8) can be transformed into (23).

$$\frac{h_{xoy} - \sin^3\theta_M}{\sin\theta_M} > 0 \tag{23}$$

As can be seen from Fig. 4, for any point P in $\boldsymbol{H}$ space, a line PB tangents to the astroid curve, and the intersection point of the tangent line and the H_{xoy} axis is $P_0(\sin\theta_M, 0)$. The tangent line PB intersects with the astroid curve at $A(\sin^3\theta_M, -\cos^3\theta_M)$. When $0 < \theta_M < \pi$, it is obvious that PA segment is in a stable state and AB segment is in an unstable state. Similarly, when $-\pi < \theta_M < 0$, PC segment is in an unstable state and CD segment is in a stable state. The stable part of the tangent line is perpendicular to the equipotential curve of the stable state. Since $de_0 = -\mu_0 \boldsymbol{m} dh_a = 0$ when the field changes along the isopotential curve, so the magnetization direction is perpendicular to the equipotential curve.

It is easier to determine the direction of magnetization by selecting the equipotential surface equation of stable magnetization state of magnetic particles as the critical surface of the operator than by selecting S-W astroid surface.

From what has been discussed above, the equipotential surface equations under magnetized stable state (when $e < -0.5$ in (10)) are selected as the critical surface formulation for anisotropic hysteresis operators. Similarly, the critical surface of isotropic hysteresis operators is formed by the equations (when $e < 0$ in the (21)). Hysteresis operator is defined as a closed domain in $\boldsymbol{H}$ space, which is convenient for numerical analysis and has certain physical significance.

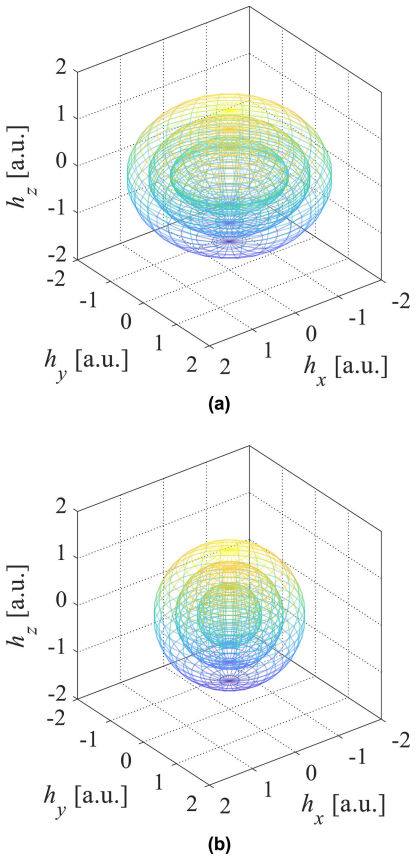

FIGURE 5. Three anisotropic hysteresis operators (a) and three isotropic hysteresis operators (b) when $e = -0.6, -1.0$, and -1.4.

Fig. 5 shows three hysteresis operators of the anisotropic and isotropic case, when $e = -0.6, -1.0$, and -1.4, respectively. Meanwhile, Fig. 5 also illustrates the effect of parameter e on the size of operators.

The relationship between h_{zmax} (the maximum of h_z along z axis) with r_{max} (the maximum radius of cross profile paralleled to xoy plane) is obtained from the analysis of Fig. 5(a). When e takes different values, the relationship of r_{max} and h_{zmax} satisfy the function $h_{zmax} = r_{max} - 0.5$. Whatever e value decreases, the longitudinal cross section of anisotropic hysteresis operator is not circular but will be infinitely close to a circle. While in Fig. 5(b), the relationship between h_{zmax} and r_{max} satisfies the function $r_{max} = h_{zmax}$ when e

takes different values. That is, no matter how the value of e decreases, the longitudinal cross section of the isotropic hysteresis operator is always circular.

Considering the principle of Preisach model, the entry point is the opening threshold, and the exit point is the closing threshold. When the applied magnetic field passes through the equipotential surface from different directions, only when $e < -0.5$ and passing through z axis is the shortest distance, which satisfies the assumption that z axis is the easy magnetization axis.

As shown in Fig. 4, for any point P in $\boldsymbol{H}$ space, the magnetization direction is perpendicular to the equipotential curve. According to these results and astroid properties in S-W model, one conclusion is obtained that the magnetization direction is depending on the locations of the applied field. When the applied field is outside of the operator's critical surface, the magnetization direction is perpendicular to the critical surface. When the magnetic field is inside the operator, the magnetization direction is fixed with the same direction as the entry point where the applied field enters the operator's critical surface. There will occur a Barkhausen jump when the applied field exits the operator's critical surface, the magnetization direction mutates to the normal direction of the tangent plane of the exit point.

The defined 3-D hysteresis operator is also in accordance with the second principle of thermodynamics, and with the loss property, congruency property, and deletion property.

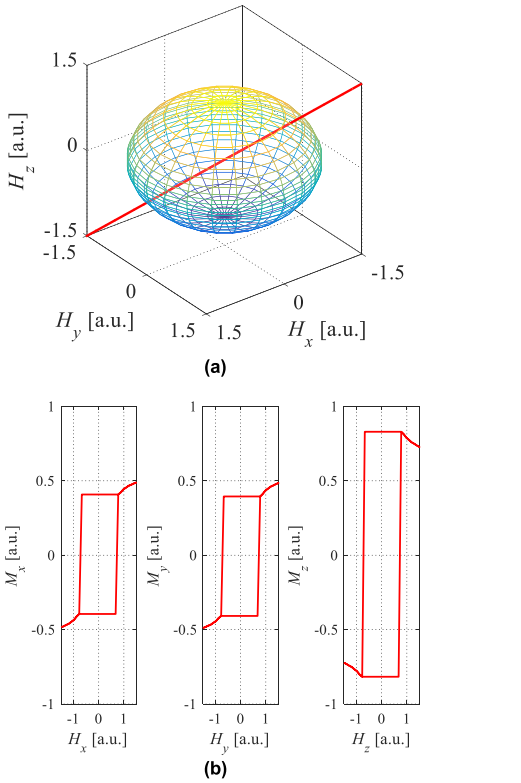

FIGURE 6. The magnetization paths (a) of a single anisotropic hysteresis operator and the corresponding hysteresis loops (b) when $e = -1$.

IV. ANALYSIS OF MAGNETIZATION PROCESS

A. ALTERNATING MAGNETIZATION

The magnetization process of anisotropic and isotropic hysteresis operators is analyzed under alternating magnetic field, respectively. The change of applied field path needs to reflect the process of entering and exiting the operator, so the setting of the maximum value of the applied field should be larger than the size of the operator. When the applied field entering the operator, the magnetization direction is fixed with the same direction as the entry point. And when the applied field exiting the operator, the magnetization direction mutates to the normal direction of the tangent plane of the exit point. Hence, when the change of the applied field from the positive maximum to the negative maximum along a certain axis and back to the positive maximum corresponds to a period of magnetization, and there will be a corresponding loop between $\boldsymbol{M}$ and $\boldsymbol{H}$.

The magnetization paths of a single anisotropic hysteresis operator and the corresponding hysteresis loops are shown in Fig. 6 when $e = -1$. And Fig. 7 shows the same case of the isotropic hysteresis operator. It is assumed that the paths of alternating magnetic field are (1.5, −1.5, −1.5) - (−1.5, 1.5, 1.5) - (1.5, −1.5, −1.5) and the hysteresis loops are given from the direction of x, y and z. The simulation steps of the operator are similar to the hysteresis modeling, which will be explained in section V.

As shown in Fig. 6, anisotropic hysteresis operators have the same hysteresis loop in the x and y directions, while that of the z direction is bigger. This is because the magnetization path inside the operator has the same projection in the x and y directions, while the z direction is slightly bigger. When the applied magnetic field crosses the critical surface of the operator, the magnetization $\boldsymbol{M}$ increases in the x and y directions, while decreases in the z direction. The reason is that as the applied magnetic field increases, the corresponding unit magnetization direction should be perpendicular to the operator's critical surface. So the component of unit magnetization increases in the x and y directions and decreases in the z direction.

As shown in Fig. 7, the hysteresis loops for isotropic operators in the x, y, and z directions can be plotted similarly. It is deduced that the magnetization $\boldsymbol{M}$ remains unchanged along with the three directions when the applied magnetic field crosses the critical surface of the operator.

In order to keep the study more general possible, more 3-D hysteresis operators are taken into account. The magnetization paths of three concentric anisotropic hysteresis operators and the corresponding hysteresis loops are shown in Fig. 8 when $e = -0.6, -1.0$, and -1.4. And Fig. 9 shows the same case of the isotropic hysteresis operator. It is assumed that the paths of alternating magnetic field are (1.5, −1.5, −1.5) - (−1.5, 1.5, 1.5) - (1.5, −1.5, −1.5).

Comparing the hysteresis loops derived from a single hysteresis operator and three ones, it can be seen that a single operator has only one jump during magnetization, while the three concentric anisotropic hysteresis operators have three

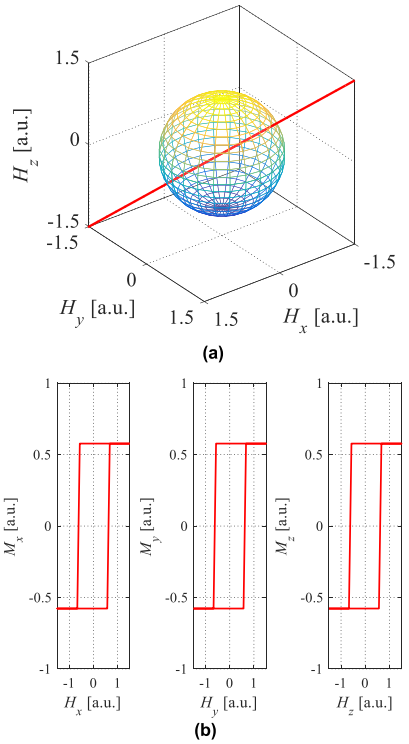

FIGURE 7. The magnetization paths (a) of a single isotropic hysteresis operator and the corresponding hysteresis loops (b) when $e = -1$.

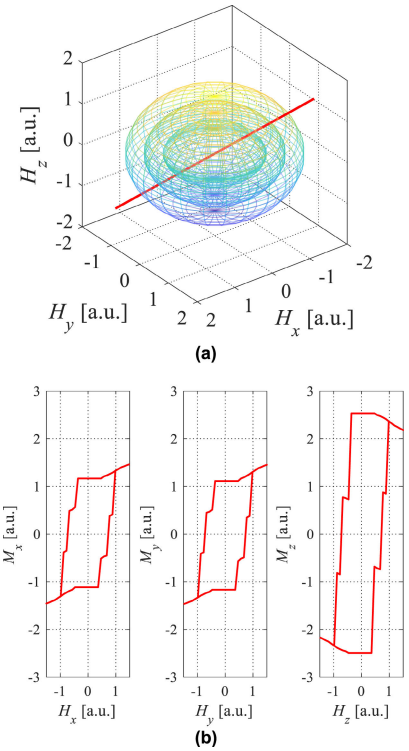

FIGURE 8. The magnetization paths (a) of three concentric anisotropic hysteresis operators and the corresponding hysteresis loops (b) when $e = -0.6, -1.0$, and -1.4.

jumps through the critical surface during the magnetization. The results show that the energy parameter e can influence the hysteresis loop.

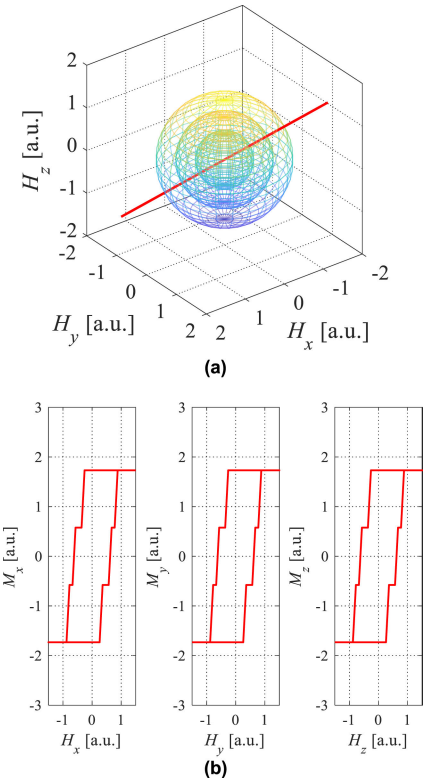

FIGURE 9. The magnetization paths (a) of three concentric isotropic hysteresis operators and the corresponding hysteresis loops (b) when $e = -0.6, -1.0$, and -1.4.

When considering the effect of the interaction field $\boldsymbol{H}_i$, the total magnetic field is equal to the vector sum of $\boldsymbol{H}_a$ and $\boldsymbol{H}_i$. The equation of equipotential surface of the hysteresis operators can be transformed to (24) and (25). So, multiple non-concentric hysteresis operators should be involved.

$$\begin{cases} h_x = H_{Ix} + \left[-\dfrac{1}{2}\sin^3\theta_M + (1-e)\sin\theta_M\right]\cos\phi \\ h_y = H_{Iy} + \left[-\dfrac{1}{2}\sin^3\theta_M + (1-e)\sin\theta_M\right]\sin\phi \\ h_z = H_{Iz} + \dfrac{1}{2}\cos^3\theta_M - \left(\dfrac{1}{2}+e\right)\cos\theta_M \end{cases} \tag{24}$$

$$\begin{cases} h_x = H_{Ix} - e\sin\theta_M\cos\phi \\ h_y = H_{Iy} - e\sin\theta_M\sin\phi \\ h_z = H_{Iz} - e\cos\theta_M \end{cases} \tag{25}$$

Three anisotropic and isotropic hysteresis operators with the effect of interaction field are considered, respectively. The alternating magnetization paths of three non-concentric anisotropic hysteresis operators and the corresponding hysteresis loops are shown in Fig. 10 when $e = -1$. And Fig.11 shows the same case of three isotropic hysteresis operators. It is assumed that the paths of alternating magnetic field are (4, −4, −1) - (−4, 4, 1) - (4, −4, −1), and $\boldsymbol{H}_i$ =2.5.

As illustrated in Fig. 10 and 11, the interaction field affects the distribution position of hysteresis operator and thereby affects the hysteresis loop. As the number of operators increases and the distribution tends to be more uniform,

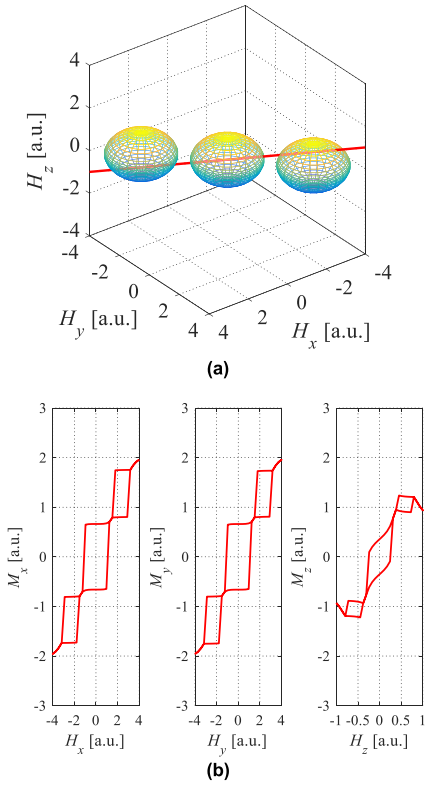

FIGURE 10. The magnetization paths (a) of three non-concentric anisotropic hysteresis operators and the corresponding hysteresis loops (b) when $e = -1$.

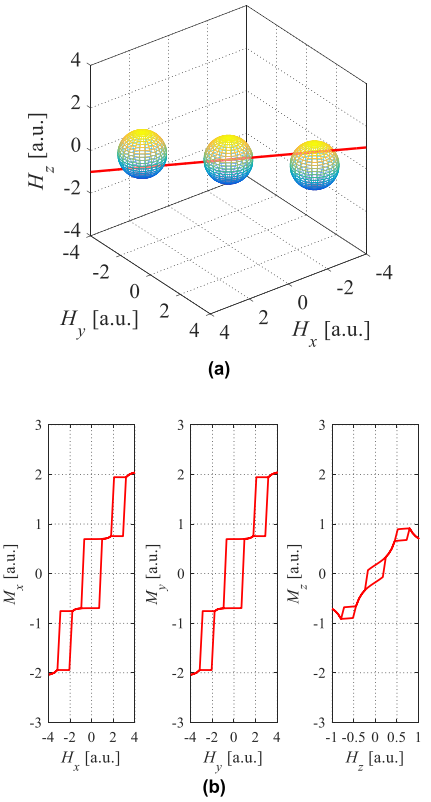

FIGURE 11. The magnetization paths (a) of three non-concentric isotropic hysteresis operators and the corresponding hysteresis loops (b) when $e = -1$.

the hysteresis loop will become more and more smooth. Therefore, once the number of operators and the distribution function is determined, the 3-D hybrid hysteresis model can be initially established. The results show the interaction field H_i can affect the hysteresis loop.

Analysis of the magnetization process shows that the factors influencing the hysteresis loop of the operator are energy parameters (related to coercive field), interaction field (affect the distribution of operators), and the number of operators.

B. ROTATIONAL MAGNETIZATION

The magnetization process of anisotropic and isotropic hysteresis operators is analyzed under rotational magnetic field. The excitation field is applied in *xoy*, *yoz* and *xoz* planes respectively. Three different sizes rotational magnetic field are applied to hysteresis operators, whose maximum magnetic field are set as 1.6, 3.2 and 4.8. The rotating direction of the rotational magnetic field is anticlockwise and $\boldsymbol{H}_i = 3.5$.

The rotational magnetization paths of five anisotropic hysteresis operators and the corresponding hysteresis loops are shown in Fig. 12. And Fig. 13 shows the same case of five isotropic hysteresis operators.

It can be seen from Fig. 12 and 13 that there has hysteresis phenomenon in the magnetization curves. When the applied field enters the critical surface of operators, the magnetization direction is frozen until it occurs barkhausen jump when the applied field exits the operator's critical surface. Conclusively, the rotational magnetization of hysteresis operator satisfies the modeling principle of hybrid vector hysteresis model.

V. PRELIMINARY STUDY AND EXPERIMENTAL VERIFICATION OF 3-D HYSTERESIS MODEL

The 3-D isotropic operator is firstly used in the 3-D modeling study due to its 3-D isotropy property. In order to simplify the calculation, the 3-D hysteresis model is regarded as the 2-D magnetization of its projection on the *xoy*, *yoz* and *xoz* planes. The previous numerical simulation method in [22] was improved by adjusting the relevant parameters and setting the cycle stop condition, and the closed magnetic characteristic curves could be obtained by the improved method.

To verify the validity of the 3-D model, the hysteresis properties of SMC material are simulated and compared with the experimental ones. The SMC material used in the experiment is SOMALOY^{TM} 500, which maximum magnetic flux density is 2.1T, and the sample is a 22mm $\times$ 22mm $\times$ 22mm cube. The measuring device used in the experiment is the 3-D magnetic properties tester [23], [24] The physical quantities measured in the experiment are the magnetic flux density and magnetic field, while what is used in the model are the magnetization and magnetic field, so the magnetic flux density $\boldsymbol{B}$ should be converted to magnetization $\boldsymbol{M}$ using (26).

$$\boldsymbol{B} = \mu_0(\boldsymbol{H} + \boldsymbol{M}) \tag{26}$$

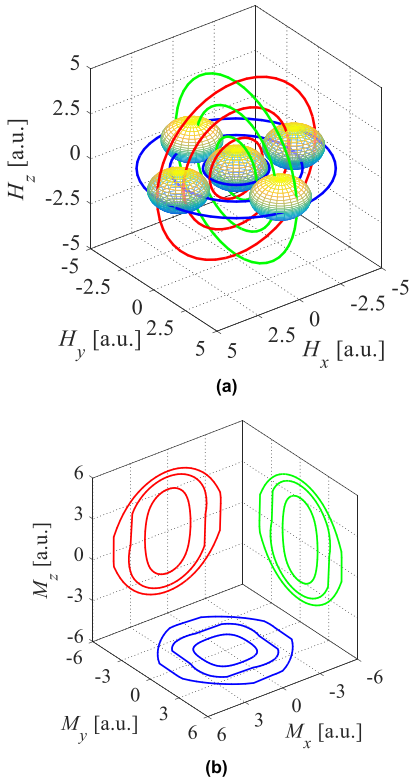

FIGURE 12. Magnetization paths (a) of five anisotropic hysteresis operators and the corresponding magnetization curves (b) when $e = -1$.

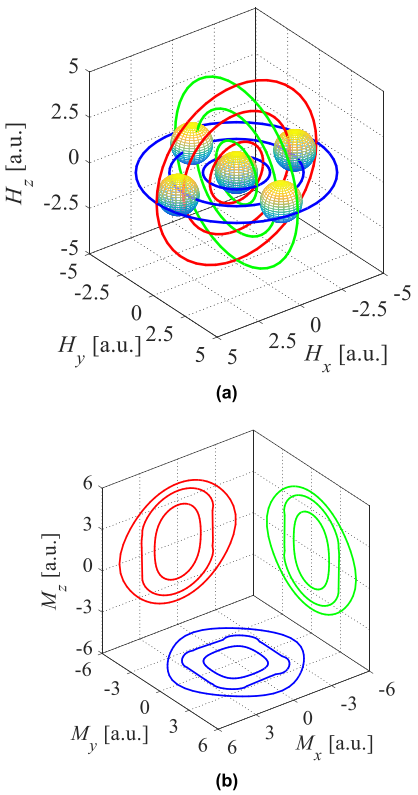

FIGURE 13. Magnetization paths (a) of five isotropic hysteresis operators and the corresponding magnetization curves (b) when $e = -1$.

where μ_0 is the permeability of vacuum, $\mu_0 = 4\pi \times 10^{-7}$ H/m.

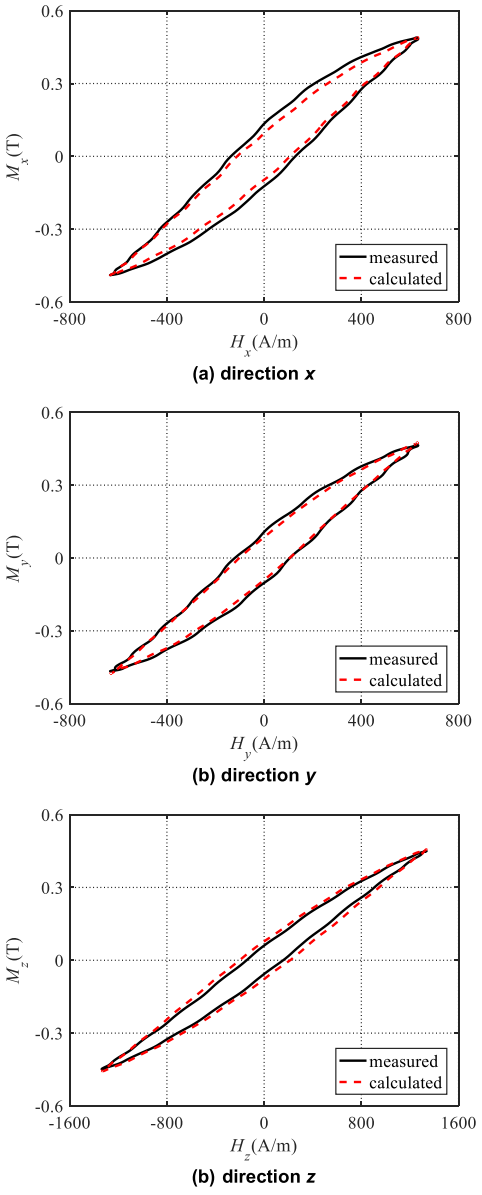

FIGURE 14. Measurement results of magnetic characteristics under 5Hz alternating magnetic field.

The magnetic characteristics of the SMC material were measured by using the 3-D magnetic tester under the condition of $B_m = 0.5$ T, 0.7 T, 1 T, 1.4 T, and 1.6 T.

By using the 3-D hysteresis model, 3-D magnetic properties of the SMC material are simulated. The main simulation steps are as follows:

(1) A three-dimensional interaction field space is defined and discretized into $n_x \times n_y \times n_z$ points, the space boundary is H_B, and the coordinate of the center point of each hysteresis operator is (H_{ix}, H_{iy}, H_{iz}).

(2) The shortest distance from the center point of the hysteresis operator (H_{ix}, H_{iy}, H_{iz}) to the space boundary H_B is set as R.

(3) The radius r considered can be obtained by discretizing the parameter R, from which the distribution law of the

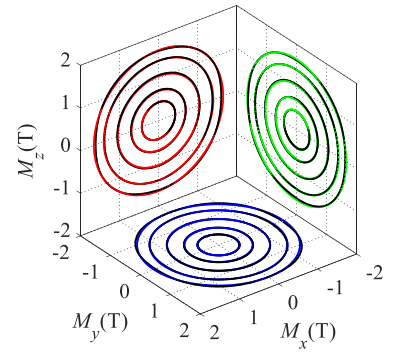

(a) The magnetization curves

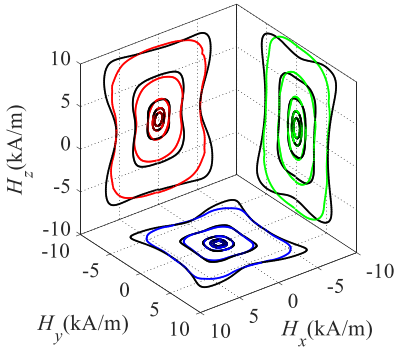

(b) The magnetic field curves

FIGURE 15. The comparison between the measurement results and simulated ones under 5Hz rotational magnetic field.

hysteresis operator can be obtained. Therefore, the number of hysteresis operators can be calculated by the equation (27). Among them, for each center point (H_{ix}, H_{iy}, H_{iz}), the value of n_r depends on the size of r and H_B. Therefore, when different sizes of external field are applied, the total number of operators is not a constant value.

$$N = \sum_{i=1}^{n_x \times n_y \times n_z} n_r\,(i) \tag{27}$$

(4) The applied external magnetic field is discretized, and the magnetization paths H_x, H_y, and H_z are obtained. When calculating the magnetization, the external field is discretized as an input.

(5) Calculating the magnetization (m_x, m_y, m_z) of each (H_x, H_y, H_z) with respect to N hysteresis operators, then the final M is the formula (28).

$$M = \frac{\sum_{j=1}^{N} m_j}{N} \times M_s \times \frac{1}{\alpha} \tag{28}$$

where M_s is the saturation magnetization of the material, and α is the correction coefficient.

According to the above steps, after converting the input external magnetic field into the output magnetization, the simulated magnetization curve can be obtained.

The alternating simulation results are compared with the experimental results, as shown in Fig. 14. The simulation result in the z direction is not better than that in the x and y directions. The reason is that the z direction is the rolling direction, it will also bring the influence of some stress factors although the material is isotropic in theory.

The rotational simulation results are compared with the experimental results, as shown in Fig. 15. The black curves in the figure are the projection of the experimental measurement results on three planes, and the color curves are the projection of the simulation results on three planes. The parameters of the model need to be determined by several groups of 3-D *B-H* data. In order to simulate hysteresis more accurately, the least square method was used to fit the correction coefficients of each group of simulation results, which can simulate the data that has not been used before. In the future, intelligent algorithms will be considered for parameter identification.

In Fig. 15(a), the simulation results are more accurate when the magnetization is low, and the simulation accuracy decreases slightly with the increase of the magnetization. As shown in Fig. 15(b), with the increase of the magnetic field intensity, the simulation accuracy decreases obviously when B_m is greater than 1 T. The reason is that the relevant parameters of operators cannot accurately reflect the real distribution of magnetic domains of the material. Further study should be carried out to optimize the parameters by means of the experimental data.

VI. CONCLUSION

This paper proposed a method for the definition of hysteresis operator in 3-D case. According to the minimum energy principle of magnetization stable state and the modeling principle of hybrid vector hysteresis model, the critical surface equations of anisotropic and isotropic hysteresis operator were given in the space sphere coordinate system, respectively. Hysteresis operator is defined as a closed surface in $\boldsymbol{H}$ space. The magnetization direction of hysteresis operator is depending on the locations of the applied field. When the applied field is outside, the magnetization direction is perpendicular to the critical surface of operators. When the applied field is inside, the magnetization direction is frozen on the direction of the entry point until it occurs barkhausen jump to the direction of the exit point.

The magnetization of anisotropic and isotropic hysteresis operators was studied under alternating and rotational magnetic field, respectively. The results show that the factors influencing the hysteresis loop of the operator are energy parameters, interaction field and the number of operators. A 3-D hysteresis model was preliminarily established based on the 3-D isotropic hysteresis operator, and the experimental verification of SMC material was carried out under different magnetic field, which verified the validity of the 3-D hysteresis operator.

REFERENCES

[1] F. Preisach, "Über die magnetische nachwirkung," *Zeitschrift Für Physik*, vol. 94, nos. 5–6, pp. 277–302, May 1935.
[2] I. D. Mayergoyz, "Mathematical models of hysteresis," *IEEE Trans. Magn.*, vol. MAG-22, no. 5, pp. 603–608, Sep. 1986.

[3] L. Chen, Q. Yi, T. Ben, Z. Zhang, and Y. Wang, "Parameter identification of Preisach model based on velocity-controlled particle swarm optimization method," *AIP Adv.*, vol. 11, no. 1, Jan. 2021, Art. no. 015022.
[4] D. C. Jiles and D. L. Atherton, "Theory of ferromagnetic hysteresis," *J. Appl. Phys.*, vol. 55, pp. 212–2115, Sep. 1984.
[5] E. C. Stoner and E. P. Wohlfarth, "A mechanism of magnetic hysteresis in heterogeneous alloys," *Philos. Trans. Roy. Soc. London A, Math., Phys. Eng. Sci.*, vol. 240, no. 826, pp. 599–642, 1948.
[6] N. Soda and M. Enokizono, "E&S hysteresis model for two-dimensional magnetic properties," *J. Magn. Magn. Mater.*, vols. 215–216, pp. 626–628, Jun. 2000.
[7] H. Hauser, "Energetic model of ferromagnetic hysteresis," *J. Appl. Phys.*, vol. 75, no. 5, pp. 2584–2597, Mar. 1994.
[8] T. Matsuo, "Anisotropic vector hysteresis model using an isotropic vector play model," *IEEE Trans. Magn.*, vol. 46, no. 8, pp. 3041–3044, Jul. 2010.
[9] G. Friedman and I. D. Mayergoyz, "Stoner-Wohlfarth hysteresis model with stochastic input as a model of viscosity in magnetic materials," *IEEE Trans. Magn.*, vol. 28, no. 5, pp. 2262–2264, Sep. 1992.
[10] C. Michelakis, G. Litsardakis, and D. Samaras, "A contribution to 2D vector Preisach modelling," *J. Magn. Magn. Mater.*, vols. 157–158, pp. 347–348, May 1996.
[11] C. Michelakis, D. Samaras, and G. Litsardakis, "A 3-D moving vectorial preisach-type hysteresis model," *J. Magn. Magn. Mater.*, vol. 207, nos. 1–3, pp. 188–192, Dec. 1999.
[12] E. D. Torre, E. Pinzaglia, and E. Cardelli, "Vector modeling—Part I: Generalized hysteresis model," *Phys. B, Condens. Matter*, vol. 372, nos. 1–2, pp. 111–114, Feb. 2006.
[13] E. D. Torre, E. Pinzaglia, and E. Cardelli, "Vector modeling—Part II: Ellipsoidal vector hysteresis model. Numerical application to a 2D case," *Phys. B, Condens. Matter*, vol. 372, nos. 1–2, pp. 115–119, Feb. 2006.
[14] E. Cardelli, E. D. Torre, and A. Faba, "A general vector hysteresis operator: Extension to the 3-D case," *IEEE Trans. Mag.*, vol. 46, no. 12, pp. 3990–4000, Dec. 2010.
[15] E. Cardelli, E. D. Torre, and A. Faba, "Properties of a class of vector hysteron models," *J. Appl. Phys.*, vol. 103, no. 7, Apr. 2008, Art. no. 07D927.
[16] E. Cardelli, E. D. Torre, and A. Faba, "Analysis of a unit magnetic particle via the DPC model," *IEEE Trans. Magn.*, vol. 45, no. 11, pp. 5192–5195, Nov. 2009.
[17] E. Cardelli, "A general hysteresis operator for the modeling of vector fields," *IEEE Trans. Magn.*, vol. 47, no. 8, pp. 2056–2067, Aug. 2011.
[18] D. Lin, P. Zhou, and M. A. Rahman, "A new anisotropic vector hysteresis model based on play hysterons," in *Proc. IEEE Int. Magnetics Conf. (INTERMAG)*, Apr. 2017, p. 1.
[19] D. D. Li, F. G. Liu, and Y. J. Li, "A new definition of the hysteron in hybrid vector hysteresis model," *Trans. China Electrotech. Soc.*, vol. 30, pp. 15–21, Jan. 2015.
[20] D. Li, F. Liu, Y. Li, Z. Zhao, C. Zhang, and Q. Yang, "Magnetic properties modeling of soft magnetic composite materials using two-dimensional vector hybrid hysteresis model," *J. Appl. Phys.*, vol. 115, no. 17, May 2014, Art. no. 17D117.
[21] D. Li, Z. Qiao, N. Yang, Y. Song, and Y. Li, "Study on vector magnetic properties of magnetic materials using hybrid hysteresis model," *CES Trans. Electr. Mach. Syst.*, vol. 3, no. 3, pp. 292–296, Sep. 2019.
[22] G. Bertotti, *Hysteresis in Magnetism: For Physicists, Materials Scientists and Engineers*. New York, NY, USA: Academic, 1998.
[23] Y. Li *et al.*, "Dynamic magnetic properties testing and analysis of the electric magnetic materials based on three-dimensional excitation structure," *Trans. China Electrotech. Soc.*, vol. 33, no. 1, pp. 166–174, 2018.
[24] C. Zhang, Y. Li, J. Li, Q. Yang, and J. Zhu, "Measurement of three-dimensional magnetic properties with feedback control and harmonic compensation," *IEEE Trans. Ind. Electron.*, vol. 64, no. 3, pp. 2476–2485, Mar. 2017.

DANDAN LI was born in Luyi, Henan, China, in 1985. She received the B.E. degree from the Anyang Institute of Technology, in 2009, and the Ph.D. degree in electrical engineering from the Hebei University of Technology, in 2015.

Since 2015, she has been a Lecturer with the School of Building Environment Engineering, Zhengzhou University of Light Industry. Her research interests include measurement and simulation of magnetic properties of materials.

ZHENYANG QIAO was born in Nanyang, Henan, China, in 1993. He received the B.E. degree in electrical engineering and automation from the Hunan University of Technology, in 2016, and the M.E. degree in electrical engineering from the Zhengzhou University of Light Industry, in 2020. He is currently pursuing the Ph.D. degree in electrical engineering with the School of Mechatronic Engineering and Automation, Shanghai University.

YUXIANG WU was born in Chengdu, Sichuan, China, in 1995. He received the B.E. degree in engineering from the Institute of Disaster Prevention, in 2018. He is currently pursuing the master's degree in electrical engineering with the School of Building Environment Engineering, Zhengzhou University of Light Industry.

ZHONGKANG LI was born in Zhumadian, Henan, China, in 1998. He received the B.E. degree in electrical engineering and automation from Liaoning Technical University, in 2019. He is currently pursuing the master's degree in electrical engineering with the School of Building Environment Engineering, Zhengzhou University of Light Industry.

YINMAO SONG was born in 1963. He received the B.E. and M.S. degrees in engineering from the Hebei University of Technology, in 1983 and 1988, respectively.

From 1988 to 2014, he worked at the College of Electrical and Information Engineering, Zhengzhou University of Light Industry. From 2000 to 2014, he was a Professor and the Vice President with the College of Electrical and Information Engineering, and the Director of the Henan Automation Society. Since 2014, he has been a President of the School of Building Environment Engineering. He is the author of two books and more than 70 articles.

YONGJIAN LI (Member, IEEE) was born in Hebei, China, in 1978. He received the B.E., M.E., and Ph.D. degrees from the Hebei University of Technology, Tianjin, China, in 2002, 2007, and 2011, respectively.

From 2009 to 2011, he was a Visiting Research Fellow with the University of Technology Sydney, Sydney, Australia. He is currently a Professor with the School of Electrical Engineering, Hebei University of Technology. His research interests include measurement magnetic properties, modeling of magnetic materials, and power electronics.